

# Dynamical Transition for a class of integrable models coupled to a bath

Madhumita Sarkar and K. Sengupta

*School of Physical Sciences, Indian Association for the Cultivation of Science,  
2A and 2B Raja S. C. Mullick Road, Jadavpur 700032, India*

(Dated: June 29, 2020)

We study the dynamics of correlation functions of a class of  $d$ -dimensional integrable models coupled linearly to a fermionic or bosonic bath in the presence of a periodic drive with a square pulse protocol. It is well known that in the absence of the bath, these models exhibit a dynamical phase transition; all correlators decay to their steady state values as  $n_0^{-(d+1)/2}$  [ $n_0^{-d/2}$ ] above [below] a critical frequency  $\omega_c$ , where  $n_0$  is the number of drive cycles. We find that the presence of a linearly coupled fermionic bath which maintains integrability of the system preserves this transition. We provide a semi-analytic expression for the evolution operator for this system and use it to provide a phase diagram showing the different dynamical regimes as a function of the system-bath coupling strength and the bath parameters. In contrast, when such models are coupled to a bosonic bath which breaks integrability of the model, we find exponential decay of the correlators to their steady state. Our numerical analysis shows that this exponential decay sets in above a critical number of drive cycles  $n_c$  which depends on the system-bath coupling strength and the amplitude of perturbation. Below  $n_c$ , the system retains the power-law behavior identical to that for the closed integrable models and the dynamical transition survives. We discuss the applicability of our results for interacting fermion systems and discuss experiments which can test our theory.

## I. INTRODUCTION

The physics of driven quantum systems has been actively studied in recent years<sup>1</sup>. Out of these, periodically driven systems host several phenomena that do not have any analog in their aperiodic driven counterparts<sup>2</sup>. For example, periodic drives may lead to generation of quantum states with non-trivial topology even when the corresponding ground state of the system is topologically trivial<sup>3</sup>. In addition, such driven systems may lead to novel steady states which are otherwise inaccessible<sup>4</sup>. Moreover, driven quantum systems can lead to stable phases of quantum matter which have no counterparts in absence of a drive; such phases may be classified based on their symmetries<sup>5</sup>. These system also exhibit the phenomenon of dynamic freezing where the starting state of the driven system displays a perfect overlap with itself at the end of one or multiple drive periods<sup>6</sup>. More recently, it was found that periodic drives may lead to weak ergodicity breaking behavior; the drive frequency may be tuned to switch between regimes displaying relatively quick thermalization consistent with eigenstate thermalization hypothesis (ETH) and long-time coherent oscillatory dynamics which constitutes example of violation of ETH in non-integrable systems without disorder<sup>7</sup>.

Such driven system also display the phenomenon of dynamical transitions which can be thought as the non-equilibrium counterparts of quantum phase transitions<sup>8,9</sup>. A class of such transition manifest themselves through cusp-like singularities in their Loschmidt echo; the origin of such singularities have been shown to be due to crossing of non-analyticities (or Fisher zeroes) of the dynamic free energy of the driven system<sup>8</sup>. Such transitions do not lead to perceptible changes in properties of local correlation functions. In contrast, the second class of transitions which is known to occur in driven

closed integrable quantum systems, manifest themselves through the approach of the local correlation functions to their steady state values<sup>9</sup>. For a  $d$ -dimensional closed integrable model after  $n_0 \gg 1$  cycles of the drive, the correlation functions are shown to decay to their steady state values as  $n_0^{-(d+2)/2}$  for high drive frequencies and as  $n_0^{-d/2}$  for low drive frequencies. These two dynamical regimes are separated by a critical drive frequency  $\omega_c$  at which the transition occurs; indeed, for  $d = 1$  models, it was shown that there could be several reentrant transition between these two regimes. The reason for this transition was analyzed in terms of Floquet Hamiltonian of such driven systems. It was shown that such transition occur due to appearance of additional extrema in the Floquet spectrum as the drive frequency is lowered<sup>9,10</sup>; in this sense, this phenomenon is analogous to first order phase transitions in equilibrium statistical mechanics where transitions occur due to appearance of additional minima in the system's free energy. However, such transition have been shown to exist for closed integrable models only; the fate of such transition in either open or interacting quantum systems where the system can be non-integrable has not been studied so far.

In this work, we study a class of  $d$ -dimensional periodically driven integrable quantum systems coupled to a fermionic or bosonic bath focussing on the fate of such dynamical transitions in the presence of these bath. These models describes a large class of spin and fermion models such as Ising model in  $d = 1$ , Kitaev model in  $d = 2$ , superconductors and charge/spin density waves (CDW/SDW) systems, and Dirac or Weyl like quasiparticles in graphene, topological insulators (TI) and Weyl semi-metals (WSM). All these systems are described by

fermionic Hamiltonian given by

$$H_0(t) = \sum_{\vec{k}} \psi_{\vec{k}}^\dagger [(g(t) - z_{\vec{k}})\tau_3 + \Delta_{\vec{k}}\tau_+ + \text{h.c.}] \psi_{\vec{k}} \quad (1)$$

where  $\psi_{\vec{k}} = (c_{\vec{k}}, c_{-\vec{k}}^\dagger)^T$  is a two component fermionic field,  $c_{\vec{k}}$  denotes fermion annihilation operator, the sum over momenta extends over half of the Brillouin zone,  $\tau_{1,2,3}$  denotes Pauli matrices in the particle-hole space, and the specific forms of  $g(t)$ ,  $z_{\vec{k}}$  and  $\Delta_{\vec{k}}$  depend on the context of the model studied. For example for the 1D Ising model,  $g(t)$  denotes the transverse magnetic field in units of the nearest neighbor interaction  $J$  between Ising spins,  $z_k = \cos k$  and  $\Delta_k = i \sin k$  (where the lattice spacing  $a$  is set to unity)<sup>11</sup>. For the 2D Kitaev model on a square lattice, depicting  $p$ -wave superconductors, with parameters  $J_{1,2,3}$  (where  $J_3$  is chemical potential for the fermions and  $J_1$  and  $J_2$  are their hopping strength and pairing amplitude respectively) and unit lattice spacing,  $z_{\vec{k}} = (\cos(k_x) + \cos(k_y))$ ,  $g(t) = J_3(t)/J_1$ , and  $\Delta_{\vec{k}} = iJ_2[\sin(k_x) + \sin(k_y)]/J_1$ <sup>12</sup>. This model is topologically equivalent to the Kitaev spin model on the honeycomb or brickwall lattices for  $J_1 = J_2$ <sup>13</sup>. We note that for Dirac quasiparticles the two component wavefunction is given by  $\psi'_{\vec{k}} = (c_{\vec{k}\uparrow}, c_{\vec{k}\downarrow})^T$  where  $\sigma = (\uparrow, \downarrow)$  denote spin (for TIs and WSMs) or pseudospin (for graphene) indices; such a wavefunction can be easily mapped to  $\psi_{\vec{k}}$  using a particle-hole transformation. A similar consideration holds for wavefunctions of CDW and SDW systems. In what follows we shall study the dynamics of such a model driven periodically by varying  $g(t)$  and coupled to a fermionic/bosonic bath. Our numerical results would use examples of 1D Ising and 2D square lattice Kitaev models for  $p$ -wave superconductors; however qualitatively similar features are expected to hold for TI, WSM, and graphene quasiparticles, Kitaev spin models on honeycomb and brick-wall lattices, and CDW/SDW systems mentioned above.

The main results that we find from such a study are as follows. First, for  $H_0$  coupled linearly to a non-interacting bath which retains the integrability of the system, we obtain an exact semi-analytic expression for the evolution operator  $U$  and hence the Floquet eigenspectrum. Using the properties of the Floquet spectrum and also via explicit calculation of dynamic behavior of system correlation functions, we show that the system displays dynamical transitions. Second, our analysis finds that the system-bath coupling strength can be tuned to induce additional dynamical transitions for high drive frequencies where the closed system always remains in the high frequency phase; such transitions have no analog in closed driven systems studied earlier. We provide a comprehensive phase diagram charting out the positions of different dynamical phases as a function of the drive frequency and the bath parameters. Third, for  $H_0$  coupled to a bosonic bath which destroys integrability of the system, we find that all correlators, at long drive times, always decay exponentially to their steady state values.

Such an exponential decay of the correlators is characterized by decay constants. We analyze these driven systems by using an equation of motion approach<sup>14</sup> and chart out the behavior of these decay constants as a function of drive frequency. Fourth, we find that such exponential decay of correlators sets in after a critical number of drive cycles  $n_c$ ; for  $n_0 \ll n_c$ , the correlation functions display power law behavior similar to their closed counterpart. We chart out the dependence of  $n_c$  on the drive amplitude and the system-bath coupling strength. Our analysis demonstrates that the dynamical transition of the closed system survives till a large number of drive cycles at weak system-bath coupling and low drive amplitude. Finally, we discuss the applicability of our analysis to weakly-interacting fermionic systems and chart out experiments which can test our theory.

The plan for the rest of the paper is as follows. In Sec. II, we discuss the dynamical transitions in the presence of a fermionic bath. This is followed by Sec. III where we chart out the fate of such transitions in the presence of a bosonic bath. Finally, we discuss our main results, chart out experiments which can test our theory, and conclude in Sec. IV.

## II. FERMIONIC BATH

In this section, we shall discuss the dynamics of the integrable models described by  $H_0$  (Eq. 1) coupled to fermionic bath. The properties of the Floquet spectrum of the system is described in Sec. II A while a phase diagram indicating different dynamical regimes is presented in Sec. II B.

### A. Floquet Hamiltonian

The total Hamiltonian for the integrable model  $H_0$  (Eq. 1) linearly coupled to fermionic bath can be written as

$$H = H_0(t) + H_{\text{int}} + H_b \quad (2)$$

where  $H_b$  is the bath Hamiltonian, and the interaction between the system and bath is modeled by  $H_{\text{int}}$ . The periodic drive is implemented via a square pulse drive protocol,

$$\begin{aligned} g(t) &= g_i, 0 \leq t < T/2 \\ &= g_f, T/2 \leq t < T \end{aligned} \quad (3)$$

where  $T = 2\pi/\omega_D$  is the time-period of the drive and  $\omega_D$  is the drive frequency. For the 1D Ising model  $g(t)$  indicates time varying magnetic field while for the Kitaev  $p$ -wave model  $g(t) = J_3(t)$ . The bath Hamiltonian is given by

$$H_b = \sum_{\vec{k}} \epsilon_b(\vec{k}) f_{\vec{k}}^\dagger f_{\vec{k}} \quad (4)$$

where  $f_{\vec{k}}^\dagger$  is the creation operator for bath fermions  $\epsilon_b(\vec{k}) = \eta \sum_{i=1,d} \cos k_i$  where  $\eta$  is a constant. Such a bath Hamiltonian constitutes the simplest possible choice of tight-binding non-interacting fermion model; in this work, we shall restrict ourselves to this model for concreteness. We choose the spatial dimension of the bath to be same as that of the system; thus for the Ising chain we choose a 1D bath with  $\epsilon_b(k) = \eta \cos(k)$  while for the Kitaev model  $\epsilon_b(\vec{k}) = \eta(\cos(k_x) + \cos(k_y))$ . The interaction between the system and the bath is described by

$$H_{\text{int}} = \sum_{\vec{k}} \left( \lambda_{\vec{k}} c_{\vec{k}} f_{\vec{k}}^\dagger + \text{h.c.} \right) \quad (5)$$

where  $\lambda_{\vec{k}}$  is the coupling function. For numerical studies on transverse field Ising chain or Kitaev model, we shall take  $\lambda_{\vec{k}} = \lambda$  to be a constant.

For the closed system, it is well known that all correlators exhibit one or multiple dynamical transition(s) as a function of the drive frequency; the critical frequency of this transition can be inferred from the eigenspectrum of its Floquet Hamiltonian<sup>9,10</sup>. Thus we compute the Floquet spectrum of the system described by  $H$  (Eq. 2) and subjected to a periodic drive given by Eq. 3. In what follows, we shall use the path-integral technique developed in Ref. 15 for computation of the Floquet Hamiltonian. In this method, one express the matrix elements of the evolution operator  $\hat{U}$  of a quantum many body system between two coherent states in imaginary time at a temperature  $T_0$ . This is followed by a Wick-rotation to real time  $\beta = 1/(k_B T_0) \rightarrow iT/\hbar$ , where  $k_B$  is the Boltzmann constant; such a rotation can be analytically done for driven Gaussian system for the protocol given in Eq. 3. This allows one to obtain  $\hat{U}$  analytically in real time; the form of the Floquet Hamiltonian can then be read off from the expression of  $\hat{U}$ . It was shown in Ref. 9 that this method reproduce the exact Floquet Hamiltonian for closed integrable Dirac systems whose Hamiltonians are given by  $H_0(t)$ .

We begin by computing the evolution operator for the system for the square pulse protocol (Eq. 3) which is given by

$$\begin{aligned} \hat{U}(T, 0) &= \hat{U}(T, T/2) \hat{U}(T/2, 0) = \hat{U}_f \hat{U}_i \\ &= e^{-iH[g_f]T/(2\hbar)} e^{-iH[g_i]T/(2\hbar)} \end{aligned} \quad (6)$$

To obtain the Floquet Hamiltonian we first compute the matrix elements of  $\hat{U}_f$  and  $\hat{U}_i$  between two arbitrary coherent states. For this we note that the two component system fields are either given by  $\psi_{\vec{k}} = (c_{\vec{k}}, d_{\vec{k}})^T$  (for CDW/SDW systems) or as  $\psi_k = (c_k, c_{-k}^\dagger)^T$  (for Ising and Kitaev models and superconductors); for the latter class, we shall follow Ref. 15 and perform a particle-hole transformation  $c_{-k}^\dagger \rightarrow d_k$  so that one can have a uniform

formalism for both the cases. No such transformations were carried out for the bath fields. Using this, and performing the Wick's rotation mentioned above we get

$$\begin{aligned} \langle \Phi_{\vec{k}}^1 | \hat{U}_{\vec{k}a} | \Phi_{\vec{k}}^2 \rangle &= \exp[-\Phi_{\vec{k}}^{1*} \mathcal{L}_{\vec{k}a} \Phi_{\vec{k}}^2] \\ \Phi_{\vec{k}}^{b*} &= (\psi_{\vec{k}}^*, \psi_{-\vec{k}}^*, \psi_{\vec{k}}^{\prime*}, \psi_{-\vec{k}}^{\prime*}) \end{aligned} \quad (7)$$

where  $b = 1, 2$ ,  $a = i, f$ ,  $\psi_{\pm\vec{k}}$  and  $\psi_{\pm\vec{k}}^{\prime}$  denotes fermionic coherent states for the system and bath respectively and  $\hat{U}_a = \prod_{\vec{k}>0} \hat{U}_{\vec{k}a}$ . Here  $\mathcal{L}$  can be written as

$$\begin{aligned} \mathcal{L}_{\vec{k}a} &= I - G_a^{-1}(\vec{k}, 0^+), \\ G_a(\vec{k}, 0^+) &= \frac{1}{\beta} \sum_{\omega_n} G_a(\vec{k}, i\omega_n) e^{-i\omega_n \eta} \end{aligned} \quad (8)$$

where  $\beta = 1/(k_B T)$  is the inverse temperature,  $I$  denotes the  $4 \times 4$  identity matrix,  $\omega_n$  denotes the Matsubara frequency, the index  $a$  takes value  $a = i, f$ , the limit  $\eta \rightarrow 0^+$  is to be taken at the end of the calculation, and  $G_{i(f)}$  denotes the Green function of the system corresponding to  $g = g_i(g_f)$  whose calculation shall be charted out later in this section. Thus we obtain the matrix element of  $\hat{U} = \hat{U}_f \hat{U}_i$  as

$$\begin{aligned} \langle \Phi_{\ell'} | \hat{U} | \Phi_{\ell} \rangle &= \langle \Phi_{\ell'} | \hat{U}_f \hat{U}_i | \Phi_{\ell} \rangle \\ &= \int D\Phi' D\Phi'^* e^{-\sum_{\vec{k}} |\Phi_{\vec{k}}'|^2 + \Phi_{\vec{k}}'^* \mathcal{L}_{\vec{k}f} \Phi_{\vec{k}}' + \Phi_{\vec{k}}'^* \mathcal{L}_{\vec{k}i} \Phi_{\ell'} \vec{k}} \\ &= \exp[-\sum_{\vec{k}} \Phi_{\ell\vec{k}}'^* \mathcal{L}_{\vec{k}f} \mathcal{L}_{\vec{k}i} \Phi_{\ell'\vec{k}}] \end{aligned} \quad (9)$$

Since  $\Phi_{\ell\vec{k}}'^*$  and  $\Phi_{\ell'\vec{k}}$  are arbitrary coherent states, one can identify the evolution operator as

$$U_{\vec{k}}(T, 0) = \mathcal{M}_{\vec{k}} = \mathcal{L}_{\vec{k}f} \mathcal{L}_{\vec{k}i}. \quad (10)$$

In particular, the eigenvalues of  $\mathcal{M}_{\vec{k}}$ ,  $\lambda_{\vec{k}n}$ , are related to those of the Floquet Hamiltonian,  $\epsilon_{\vec{k}n}^F$  as<sup>15</sup>

$$\lambda_{\vec{k}n} = \exp[-i\epsilon_{\vec{k}n}^F T/\hbar]. \quad (11)$$

Next, we chart out the computation of  $G_{i(f)}(0^+)$ . To this end, we write the action corresponding to  $H$  (after the particle-hole transformation discussed earlier in the section) as<sup>16</sup>

$$S[\Phi^*, \Phi] = \int_0^\beta d\tau (\Phi^* I \partial_\tau \Phi + H_a[\Phi^*, \Phi]) \quad (12)$$

where  $\Phi$  is the four component field and  $H_a$  denotes the full Hamiltonian (Eq. 2) with  $g = g_a$  and  $a = i, f$ . Using Eq. 12, one obtains

$$G_a^{-1}(\vec{k}, \omega_n) = - \begin{pmatrix} i\omega - \epsilon[\vec{k}; g_a] & -\Delta_{\vec{k}} & -\lambda_{\vec{k}} & 0 \\ -\Delta_{\vec{k}} & \epsilon[\vec{k}; g_a] + i\omega & 0 & -\lambda_{\vec{k}} \\ -\lambda_{\vec{k}}^* & 0 & i\omega - \epsilon_b(\vec{k}) & 0 \\ 0 & -\lambda_{\vec{k}}^* & 0 & \epsilon_b(\vec{k}) + i\omega \end{pmatrix} \quad (13)$$

where  $\epsilon[\vec{k}; g_a] = g_a - z_{\vec{k}}$ . Using Eq. 13, it is easy to find  $G_a(\vec{k}, \omega_n)$ . In particular we find that poles of these equations, assuming  $\lambda_{\vec{k}}$  to be real, are given by the solution of the equation

$$\omega_n^4 + \omega_n^2(\Delta_{\vec{k}}^2 + \epsilon[\vec{k}; g_a]^2 + \epsilon_b^2(\vec{k}) + 2\lambda_{\vec{k}}^2) + \Delta_{\vec{k}}^2\epsilon_b^2(\vec{k}) + \epsilon^2[\vec{k}; g_a]\epsilon_b^2(\vec{k}) + \lambda_{\vec{k}}^4 - 2\epsilon[\vec{k}; g_a]\epsilon_b(\vec{k})\lambda_{\vec{k}}^2 = 0 \quad (14)$$

and are given by  $\omega_{1..4} = \pm\sqrt{\alpha_{\vec{k}} \pm \sqrt{\beta_{\vec{k}}}}$ , where

$$\begin{aligned} \alpha_{\vec{k}} &= [\Delta_{\vec{k}}^2 + 2\lambda_{\vec{k}}^2 + \epsilon^2[\vec{k}; g_a] + \epsilon_b^2(\vec{k})]/2 \\ \beta_{\vec{k}} &= [\Delta_{\vec{k}}^2 + 2\lambda_{\vec{k}}^2 + \epsilon^2[\vec{k}; g_a] + \epsilon_b^2(\vec{k})]^2/4 \\ &\quad - [\Delta_{\vec{k}}^2\epsilon_b^2(\vec{k}) + \lambda_{\vec{k}}^4 + \epsilon^2[\vec{k}; g_a]\epsilon_b^2(\vec{k}) - 2\lambda_{\vec{k}}^2\epsilon[\vec{k}; g_a]\epsilon_b(\vec{k})] \end{aligned} \quad (15)$$

Using Eq. 14 one obtains

$$G_a(\vec{k}, \omega_n) = \prod_{i=1,4} (i\omega_n - \omega_i)^{-1} \mathcal{C}_a(\vec{k}, \omega_n) \quad (16)$$

where  $\mathcal{C}_a$  denotes the adjoint of the cofactor matrix of  $G_a^{-1}$ . From Eq. 16, one can compute

$$G_a(\vec{k}, 0^+) = \sum_{i=1,4} \frac{[1 - n_F(\omega_i)]\mathcal{C}_a(\vec{k}, \omega_i)}{\prod_{j \neq i, j=1,4} (\omega_i - \omega_j)} \quad (17)$$

where  $\omega_i$  are the poles of the Greens's function (Eq. 16) and  $n_F(\omega_i) = (1 + \exp[\beta\omega_i])^{-1}$  is Fermi-Dirac distribution function. This allows us to obtain expression for  $\mathcal{L}_{\vec{k}a} = I - [G_a(\vec{k}, 0^+)]^{-1}$  and subsequently  $\mathcal{M}_{\vec{k}}$  using Eq. 17 and 8. This leads to the Floquet eigenvalues  $\epsilon_{\vec{k}n}^F$  (Eq. 11).

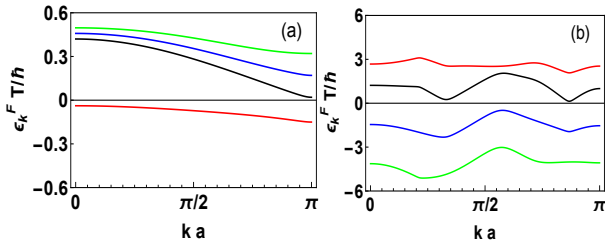


FIG. 1: Plot of Floquet eigenvalues  $\epsilon_{\vec{k},n}^F T/\hbar$  for 1D Ising model as a function of  $k$  for  $n = 1..4$ . (a)[(b)] shows their dispersion at high [low] frequency  $\omega_D = 10[0.2]\pi$ . For all plots,  $g_f = 2$ ,  $g_i = 0$ , and both the lattice spacing  $a$ , and the Ising interaction strength  $J$  is set to unity.

A plot of the Floquet eigenvalues for Ising model in a transverse field is shown in Fig. 1. Here the lattice spacing  $a$  and the Ising interaction strength  $J$  is set to unity,  $z_k = \cos(k)$ ,  $\Delta_k = i \sin(k)$ ,  $g_f/J = 2$ ,  $g_i/J = 0$ , and we have chosen representative values  $\lambda/J = 0.8$  and  $\eta/J = 0.1$  for these plots. Fig. 1(a) shows  $\epsilon_{\vec{k},n}^F T/\hbar$  as a function of  $k$  for  $\omega_D = 10\pi$  while Fig. 1(b) shows the corresponding plot at  $\omega_D = 0.2\pi$ . We find that at low frequency Floquet eigenvalues display multiple extrema as shown in the Fig. 1(b); this is in sharp contrast to their behavior at high frequency shown in Fig. 1(a) where the extrema are only found at  $k = 0, \pi$ . This behavior indicates the possibility of a dynamical transition at finite  $\lambda$  and  $\eta$ ; this will be discussed in details in Sec. II B.

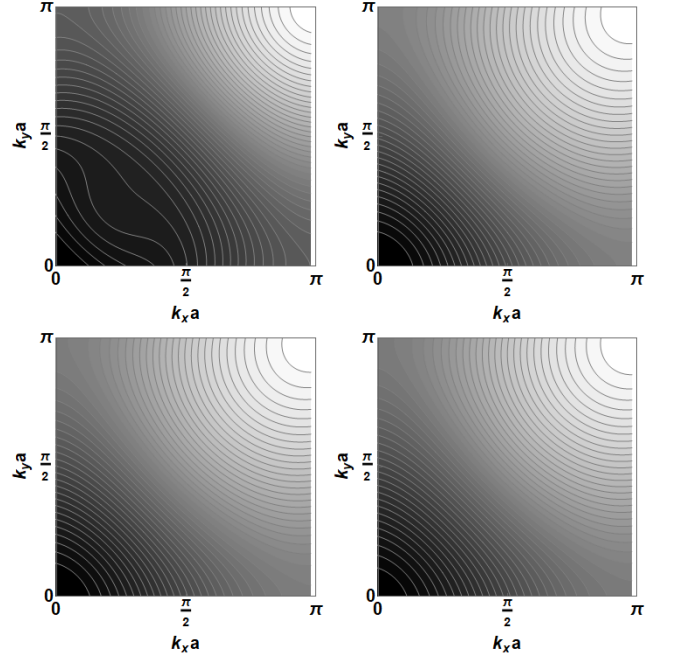


FIG. 2: Plot of Floquet eigenvalues  $\epsilon_{\vec{k}}^F T/\hbar$  for 2D Kitaev model as a function of  $\vec{k} = (k_x, k_y)$ . Each panel corresponds to one of the eigenvalues (four in total). For all plots,  $\hbar\omega_D/J_1 = 10\pi$ ,  $g = J_3$  with  $g_f = 5J_1$  and  $g_i = 4J_1$ ,  $\lambda = 0.8J_1$ ,  $\eta = 0.1J_1$ ,  $J_2 = J_1 = 1$  and the lattice spacing  $a$  is set to unity. The white (black) regions denote high (low) values. See text for details.

Similar plots for the Floquet eigenvalues for the 2D Kitaev model in the gapped phase is shown in Figs. 2 and

3. For the Kitaev model,  $\Delta_{\vec{k}} = J_2 i(\sin(k_x a) + \sin(k_y a))$ ,  $z_{\vec{k}} = J_1(\cos(k_x a) + \cos(k_y a))$ ,  $J_3(t)/J_1 = g(t)$ , and  $a$  is the lattice spacing. Here, we have chosen  $J_1 = J_2 = 1$ ,  $J_{3f} = 5J_1$ ,  $J_{3i} = 4J_1$ ,  $\lambda = 0.8J_1$  and  $\eta = 0.1J_1$ . Figs. 2 and 3 display four Floquet eigenvalues at  $\hbar\omega_D/J_1 = 10\pi$  and  $\hbar\omega_D/J_1 = 3.3\pi$  respectively. We find that at high frequency ( $\hbar\omega_D/J_1 = 10\pi$ ), all the Floquet eigenvalues show extrema at the band edges or center (Fig. 2); in contrast, one finds an arc of maxima for three of the four eigenvalues at low frequency ( $\hbar\omega_D/J_1 = 0.2\pi$ ). As we shall see in the next section, this behavior also indicates the existence of an intermediate dynamical transition between the high and the low frequency phases.

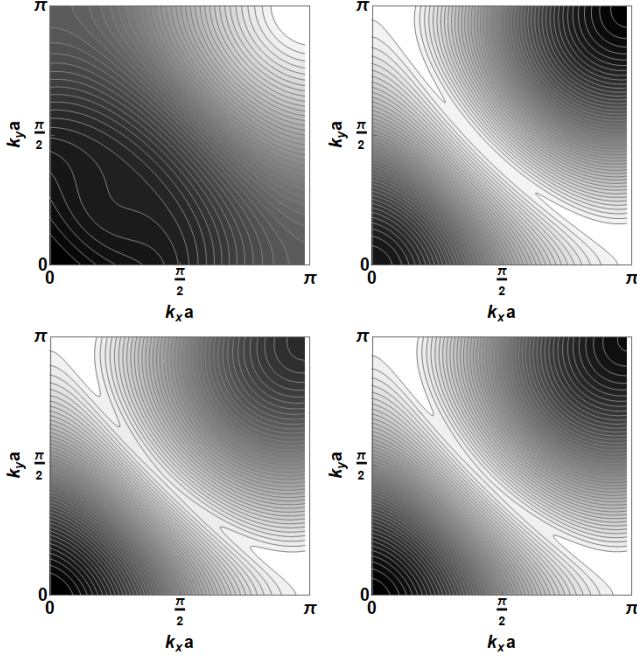


FIG. 3: Plot of Floquet eigenvalues  $e_{\vec{k}}^F T/\hbar$  for 2D Kitaev model as a function of  $\vec{k} = (k_x, k_y)$ . Each panel corresponds to one of the eigenvalues (four in total). For all plots,  $\hbar\omega_D/J_1 = 3.3\pi$ . All other parameters are same as in Fig. 2. See text for details.

## B. Phase Diagram

In this section, we chart out the different dynamical regimes of the system. It is well-known that for the closed system ( $\lambda = 0$ ), both the Ising and the Kitaev model exhibits two different dynamical regimes depending on the drive frequency<sup>9,10</sup>. For high drive frequencies, all the non-trivial correlators  $C_1(\vec{k}, n_0, T) = \langle \psi_{\vec{k}}(n_0 T) | c_{\vec{k}}^\dagger c_{\vec{k}} | \psi_{\vec{k}}(n_0 T) \rangle$ ,  $C_2(\vec{k}, n_0, T) = \langle \psi_{\vec{k}}(n_0 T) | c_{-\vec{k}}^\dagger c_{-\vec{k}} | \psi_{\vec{k}}(n_0 T) \rangle$ , and  $C_3(\vec{k}, n_0, T) = \langle \psi_{\vec{k}}(n_0 T) | c_{\vec{k}}^\dagger c_{-\vec{k}}^\dagger | \psi_{\vec{k}}(n_0 T) \rangle$  decay to their steady state values (reached as  $n_0 \rightarrow \infty$ ) as  $n_0^{-(d+1)/2}$ . In contrast, for low drive frequencies, they decay as  $n_0^{-d/2}$ . These two regimes are separated by several reentrant phase transitions at specific critical frequencies for the Ising model in  $d = 1$ ; for the Kitaev model, there is a single phase transition occurring as the drive frequency is lowered. The aim of the present section is to study the fate of these dynamical regime when  $\lambda \neq 0$ .

To understand why such a transition occur and to decipher its relation with the structure of the Floquet eigenvalues, we first rewrite the correlators in terms of the eigenvectors  $|\psi_m^F\rangle = \prod_{\vec{k}} |\psi_{\vec{k}m}^F\rangle$  and eigenvalues  $\exp[-i\epsilon_{\vec{k}m}^F T/\hbar]$  of  $U_{\vec{k}}(T, 0)$  using Eqs. 10. In terms of these, the wavefunction after  $n_0$  drive cycles and for an initial starting state  $|\psi_{\vec{k}}(0)\rangle$ , can be written as

$$|\psi_{\vec{k}}(n_0)\rangle = \sum_{m=1..4} e^{-in_0\epsilon_m^F T/\hbar} \alpha_m |\psi_{m\vec{k}}^F\rangle \quad (18)$$

where  $\alpha_m(\vec{k}) = \langle \psi_{m\vec{k}}^F | \psi_{\vec{k}}(0) \rangle$  and we have used the representation of  $U$  in terms of its eigenvalues and eigenvectors. Using this one can obtain

$$\begin{aligned} \delta C_i(\vec{k}, n_0, T) &= \sum_{m_1 \neq m_2} \alpha_{m_1}^*(\vec{k}) \alpha_{m_2}(\vec{k}) \chi_i^{m_1 m_2}(\vec{k}) e^{in_0(\epsilon_{m_1}^F(\vec{k}) - \epsilon_{m_2}^F(\vec{k}))T/\hbar} = \sum_{m_1, m_2} f_i^{m_1 m_2}(\vec{k}, n_0, T) e^{in_0(\epsilon_{m_1}^F(\vec{k}) - \epsilon_{m_2}^F(\vec{k}))T/\hbar} \\ \chi_i^{m_1 m_2}(\vec{k}) &= \langle \psi_{m_1 \vec{k}}^F | \mathcal{O}_i(\vec{k}) | \psi_{m_2 \vec{k}}^F \rangle \end{aligned} \quad (19)$$

where  $\delta C_i = C_i - C_i^{\text{steady state}}$  and  $i = 1, 2, 3$ . Here  $\mathcal{O}_1 = c_{\vec{k}}^\dagger c_{\vec{k}}$ ,  $\mathcal{O}_2 = c_{-\vec{k}}^\dagger c_{-\vec{k}}$ , and  $\mathcal{O}_3 = c_{\vec{k}}^\dagger c_{-\vec{k}}^\dagger$ . This indicates that in real space, these correlation functions can be written

as

$$\delta C_i(\vec{r}, n_0, T) = \frac{1}{2} \int \frac{d^d k}{(2\pi)^d} e^{i\vec{k} \cdot \vec{r}} \delta C_i(\vec{k}, n_0, T) \quad (20)$$

To see the behavior of  $\delta C_i$  at large  $n_0$ , we note that for any function  $f_i(k)$  and for large integer  $n_0$ , one has the

identity

$$\int f_i(\vec{k}) e^{i n_0 \phi(\vec{k})} d^d k \approx e^{i n_0 \phi(\vec{k}_0)} (n_0 \phi''(\vec{k}_0))^{-\frac{d}{2}} \times e^{\frac{\pi i \mu}{4}} \left( f_i(\vec{k}_0) + i \frac{f''(\vec{k}_0)}{2 \phi''(\vec{k}_0) n_0} + O(1/n_0^2) \right) \quad (21)$$

where  $\vec{k}_0$  is the saddle point such that  $\phi'(\vec{k}_0) = 0$ . We find that the leading behavior of this integral will be  $\sim n_0^{-d/2}$  if  $f_i(\vec{k}_0) \neq 0$  and  $\sim n_0^{-(d+2)/2}$  otherwise. Using this identity, we find that the behavior of the correlators  $\delta C_i$  comes from the saddle points of the difference of Floquet eigenvalues which we denote by  $\epsilon_k^F$ . For saddle points at high frequencies, it may be possible that  $f_i^{m_1, m_2}(\vec{k}_0^F, n_0, T) = 0$  for all  $m_1$  and  $m_2$ . This typically happens when these saddles occur at the center or edge of the Floquet Brillouin zone and leads to a  $1/n_0^{(d+2)/2}$  decay of the correlators. At lower frequencies, the contribution of the correlators comes from the saddles which are not necessarily at the zone edge or center and these lead to  $1/n_0^{d/2}$  decay of the correlators. The transition between these two phases occur at the critical frequency where an extrema first occurs in the Floquet spectrum away from the zone edge or center. This transition was shown to exist for the closed system for both Ising and Kitaev model in Ref. 9. Here we are going to numerically investigate its fate in the presence of a fermionic bath.

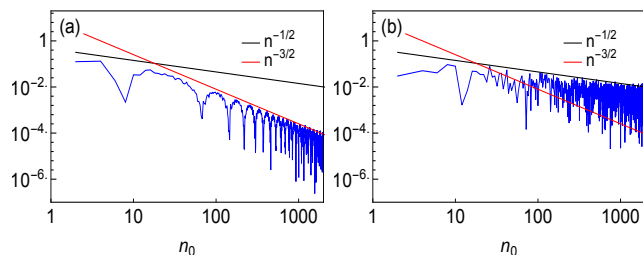


FIG. 4: Plot of the correlator  $\delta C_1(\vec{r} = 0, n_0, T)$  as a function of  $n_0$  for (a)  $\omega_D = 10\pi$  and (b)  $\omega_D = 0.2\pi$  for the 1D Ising model. For both plots,  $g_f = 2$ ,  $g_i = 0$ ,  $\lambda = 0.8$ , and  $\eta = 0.1$ . All energies(frequencies) are in units of  $J(J/\hbar)$ . See text for details.

To this end, we first consider the 1D Ising model, where we show the evolution of  $\delta C_1(\vec{r} = 0, n_0, T)$  as a function of  $n_0$  in Fig. 4 for (a)  $\hbar\omega_D/J = 10\pi$  and (b)  $\hbar\omega_D/J = 0.2\pi$ . For the plot we have chosen  $g_f/J = 2$ ,  $g_i = 0$ ,  $\lambda/J = 0.8$  and  $\eta/J = 0.1$ . Fig. 4 clearly demonstrate two dynamical regimes; in the high frequency regime, the correlators decay to their steady state value as  $n_0^{-3/2}$  while for the low-frequency phase, they have a  $n_0^{-1/2}$  behavior. This shows that the different dynamical regimes persists in the presence of fermionic bath for the 1D Ising system. We have checked that similar behavior is seen for both  $\delta C_2$  and  $\delta C_3$ .

The corresponding phase diagram displaying the two different dynamical regimes is shown in Fig. 5. Fig.

5(a) shows these regimes as a function of  $g_f$  and  $\omega_D$  for  $\eta = 0.1J$  and  $\lambda = 0.8J$ . The plot demonstrates the presence of dynamical transition for finite  $\lambda$ . We note that in the presence of finite  $\lambda$  and  $\eta$ , one needs a finite critical drive amplitude  $g_f = g_{fc} \simeq 0.9J$  for the transition to occur; for  $g_f < g_{fc}$  only the low frequency regime with  $\delta C_i \sim n_0^{-1/2}$  survives. Furthermore, for a small window of  $1.1 \leq g_f \leq 1.2$ , we find the presence of reentrant transitions as a function of  $\omega_D$  with the second transition taking place around  $\hbar\omega_D \sim 0.9J$ . Fig. 5(b) shows the position of these dynamical regimes in the  $\lambda - \omega_D$  plane for a fixed  $\eta = 0.1J$ ,  $g_f = 2J$  and  $g_i = 0$ . We note that the presence of a small  $\lambda$  leads to  $n_0^{-1/2}$  decay of the correlators even when the closed system at  $\lambda = 0$  exhibits  $n_0^{-3/2}$  behavior. This can be further understood by noting the behavior of the Floquet eigenvalues for the Ising model; the extrema of these eigenvalues shifts from  $\pi$  for infinitesimal  $\lambda$  as shown in Fig. 6. Up on increasing  $\lambda$ , the extrema returns to  $\pi$  for  $\lambda/J \simeq 0.45$  for  $\hbar\omega_D/J \geq 1.8\pi$  as can be seen from Fig. 6; this leads to the presence of dynamical transition at large enough  $\lambda$  even when the small  $\lambda$  regime has no such transition. Moreover, one finds that at high frequencies  $\hbar\omega_D/J \geq 1.8\pi$ , it is possible to have multiple transitions between the two dynamical regimes by tuning the coupling to the bath at a fixed frequency; this phenomenon has no analog in closed system studied earlier.

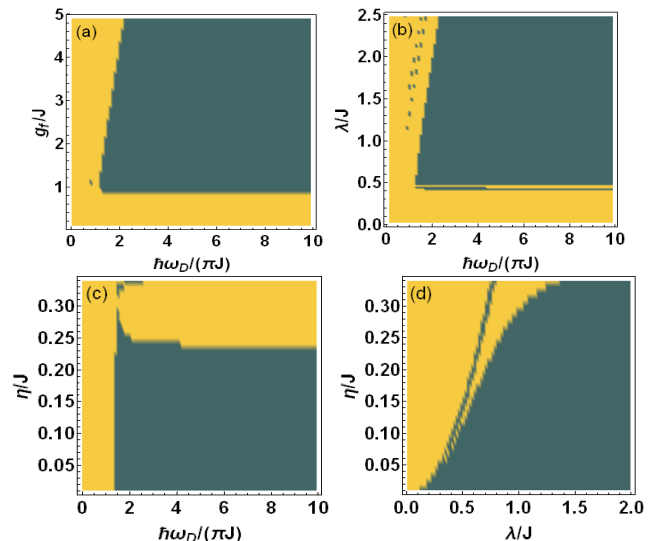


FIG. 5: (a) Plot of different dynamical regimes as a function of  $g_f/J$  and  $\hbar\omega_D/(\pi J)$  for  $\lambda = 0.8J$  and  $\eta = 0.1J$ . The green [yellow] region corresponds to  $n_0^{-3/2}$  [ $n_0^{-1/2}$ ] behavior of the correlators. (b) Plot of the dynamical regimes as a function of  $\lambda/J$  and  $\hbar\omega_D/(\pi J)$  for  $\eta = 0.1J$  and  $g_f = 2J$ . (c) Plot of the dynamical regimes as a function of  $\eta/J$  and  $\hbar\omega_D/(\pi J)$  for  $\lambda = 0.8J$  and  $g_f = 2J$ . (d) Plot of the dynamical regimes as a function of  $\eta/J$  and  $\lambda/J$  for  $\hbar\omega_D/(\pi J) = 10$  and  $g_f = 2J$ . For all plots  $g_i = 0$  and  $J = 1$ . See text for details.

Fig. 5(c) demonstrate the dependence of these regimes

on  $\eta$  and  $\omega_D$  for  $g_f = 2J$ ,  $g_i = 0$ , and  $\lambda = 0.8J$ . We find that there is a wide range of  $\eta$  for which the transition is stable.

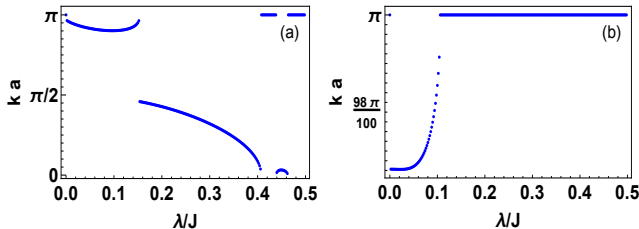


FIG. 6: The position of extrema of two of the Floquet eigenvalues as a function of  $\lambda/J$  for  $\eta = 0.1J$ ,  $g_f = 2J$ ,  $g_i = 0$ , and  $\hbar\omega_D/J = 10\pi$ . The other two eigenvalues always show extrema at  $k = \pi/a$ . In the plot, in case of multiple extrema, the one with the highest momenta other than  $\pi/a$  is shown. For all plots,  $J = a = 1$ .

Finally we chart out the position of these dynamical regimes in the  $\eta - \lambda$  plane for a fixed drive frequency  $\hbar\omega_D = 10\pi J$ ,  $g_f = 2J$ , and  $g_i = 0$  in Fig. 5(d). We find the presence of both dynamical regimes as a function of  $\eta$  and  $\lambda$  and multiple transition curves separating them. We note that only the regime with  $n_0^{-1/2}$  behavior persists for small  $\lambda$  which is consistent with the behavior of the Floquet eigenvalues in Fig. 6.

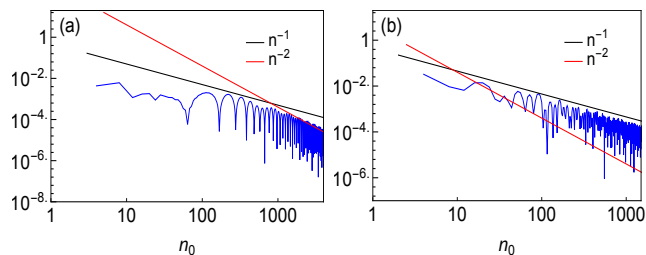


FIG. 7: Plot of  $\delta C_1$  as a function of  $n_0$  for  $\eta = 0.1J_1$ ,  $J_{3f} = 5J_1$ ,  $J_{3i} = 4J_1$ ,  $\lambda = 0.8J_1$  and  $\hbar\omega_D/(\pi J_1) = 10[3.3]$  for (a)[(b)]. For all plots,  $J_1 = J_2 = 1$ . See text for details

Next, we chart out the phase diagram for the Kitaev model. To this end, in Fig. 7, we plot  $\delta C_1(n_0, T)$  as a function of  $n_0$  for  $\hbar\omega_D/J_1 = 10\pi$  (Fig. 7(a)) and  $\hbar\omega_D/J_1 = 3.3\pi$  (Fig. 7(b)),  $\lambda/J_1 = 0.8$ ,  $J_2/J_1 = 1$ ,  $J_{3f[i]}/J_1 = 4[5]$ , and  $\eta/J_1 = 0.1$ . We find that Fig. 7(a) shows a  $1/n_0^2$  decay while Fig. 7(b) exhibits  $1/n_0$  behavior; this constitutes a clear signature of dynamical transition for finite  $\lambda$  and  $\eta$ . We have checked that the behavior of  $\delta C_2$  and  $\delta C_3$  are similar to  $\delta C_1$ .

The phase diagram displaying different dynamical regimes is exhibited in Fig. 8. In all of these plots we choose  $J_2 = J_1$  and  $J_{3i}/J_1 = 4$ . Fig. 8(a) shows the dynamical regimes as a function of  $J_{3f}/J_1 \equiv g_f$  and  $\hbar\omega_D/(\pi J_1)$  for  $\eta/J_1 = 0.1$  and  $\lambda/J_1 = 0.8$ . We find that for a distinct range of  $J_{3f}$ , the system displays both  $1/n_0^2$  (green regions) and  $1/n_0$  (yellow regions) behav-

ior. This constitutes examples of dynamical transition. In Fig. 8(b), we chart out these dynamical regimes as a function of  $\lambda/J_1$  and  $\hbar\omega_D/(\pi J_1)$  for  $J_{3f}/J_1 = 5$  and  $\eta/J_1 = 0.1$ . We find that the  $1/n_0^2$  behavior can only be seen within a finite range  $0.75 \leq \lambda/J_1 \leq 0.92$ . The extent of this region depends on  $\eta/J_1$ ; it becomes wider with larger  $\eta$ . In Fig. 8(c), we plot the dynamical regimes as a function of  $\eta/J_1$  and  $\hbar\omega_D/(\pi J_1)$  for  $\lambda/J_1 = 0.8$  and  $J_{3f}/J_1 = 5$ . We find that for  $\lambda/J_1 = 0.8$  there is a narrow region in  $\eta$  where  $1/n_0^2$  behavior survives. Finally Fig. 8(d), we plot the position of these dynamical regimes in the  $\eta - \lambda$  plane for  $\hbar\omega_D/(\pi J_1) = 10$  and  $J_{3f}/J_1 = 5$ . We find that increasing  $\eta$  shifts the presence of the dynamical regime with  $1/n_0^2$  behavior to higher values of  $\lambda$ ; it also makes it extent wider. Furthermore, for small  $\eta/J_1$ , a larger  $\lambda/J_1 > 0.8$  allows presence of  $1/n_0^2$  decay of correlators. Also, we find that increasing  $\eta$  with  $\lambda/J_1 > 0.8$  leads to reentrant transition between the two dynamical regimes; these transitions do not have any analogue in closed systems studied earlier in Ref. 9,10.

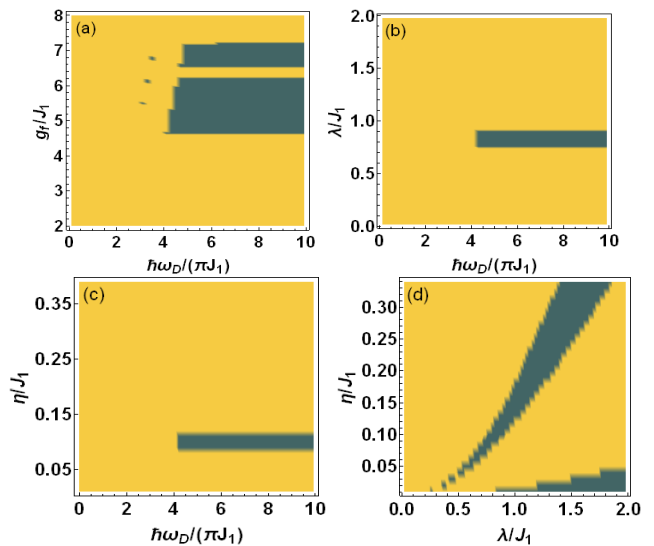


FIG. 8: (a) Plot of different dynamical regimes as a function of  $J_{3f}/J_1 \equiv g_f$  and  $\hbar\omega_D/(\pi J_1)$  for  $\lambda = 0.8J_1$  and  $\eta = 0.1J_1$ . The green [yellow] region corresponds to  $n_0^{-2}$  [ $n_0^{-1}$ ] behavior of the correlators. (b) Plot of the dynamical regimes as a function of  $\eta/J_1$  and  $\hbar\omega_D/(\pi J_1)$  for  $\lambda = 0.8J_1$  and  $J_{3f} = 5J_1$ . (c) Plot of the dynamical regimes as a function of  $\lambda/J_1$  and  $\hbar\omega_D/(\pi J_1)$  for  $\eta = 0.1J_1$  and  $J_{3f} = 5J_1$ . (d) Plot of the dynamical regimes as a function of  $\eta/J_1$  and  $\lambda/J_1$  for  $\hbar\omega_D/(\pi J_1) = 10$  and  $J_{3f} = 5J_1$ . For all plots  $J_{3i} = 4J_1$  and  $J_2 = J_1$ . See text for details.

### III. BOSONIC BATH

In this section we couple  $H_0$  to a bosonic bath. The technique used for obtaining our result is detailed in Sec. III A while the numerical results are presented in Sec. III B.

### A. Equation of motion

In the presence of a bosonic bath, the total Hamiltonian of the system reads

$$H_{\text{total}} = H_0(t) + H'_b + H'_{\text{int}} \quad (22)$$

where the bath Hamiltonian, modeled by a bunch of harmonic oscillators, is given by

$$H'_b = \sum_{\vec{q}} \hbar\omega_{\vec{q}} b_{\vec{q}}^\dagger b_{\vec{q}}. \quad (23)$$

Here  $b_{\vec{q}}^\dagger$  is creation operator for bosons and  $\omega_{\vec{q}}$  is the corresponding frequency. The interaction between the Fermions and the bath is given by

$$H'_{\text{int}} = \sum_{\vec{k}\vec{q}} \lambda_{\vec{k}} c_{\vec{k}}^\dagger c_{\vec{k}+\vec{q}} (b_{\vec{q}}^\dagger + b_{-\vec{q}}) + \text{h.c.} \quad (24)$$

where  $\lambda_{\vec{k}}$  is the coupling function which determines the strength of interaction between the system fermions and the bath bosons. Here, and in rest of this section, we shall extend definitions of  $c_{\vec{k}}$  and  $c_{-\vec{k}}$  over the entire Brillouin zone for convenience; the double counting which arises due to such an extension can be simply offset by a factor of 1/2 while evaluating sum over momentum for computing any correlation functions.

We note that the interaction between the bosonic bath and the fermions (Eq. 24) necessarily destroys integrability of the fermion system upon integrating the bath degrees of freedom. This is in contrast to the case of fermionic bath studied earlier and, as we shall see, leads to qualitative difference in the dynamics of correlators of the driven model. In what follows, we shall study the dynamics of  $H_{\text{total}}$  ignoring backreaction of the system to the bath<sup>17</sup>. This approximation has been widely used in treating such open quantum systems; it produces

accurate results for system dynamics when the bath is either very large compared to the system size or if the bath frequencies are much larger compared to the system energy scales. In what follows we shall restrict ourselves to the latter case ( $\hbar\omega_{\vec{q}}$  being the largest energy scale) and assume a thermal distribution for the bath bosons with a fixed temperature  $T_b$  at all times:  $n^b[\omega_{\vec{q}}] = (\exp[\hbar\omega_{\vec{q}}/(k_B T_b)] - 1)^{-1}$ . We also note that in this limit it is possible to integrate out the bath degrees of freedom and obtain an effective static interaction between the fermions with strength  $\sim \lambda^2/(\hbar\omega_{\vec{q}})$ ; thus our analysis also yields information about dynamics of interacting driven fermions.

To study the dynamics, we note that since the fermionic system, in the presence of the bath does not reduce to Gaussian action, the path integral procedure of the previous section can not be applied here in a straightforward manner and we need to resort to some approximation scheme. To this end, we use the equation of motion approach where one writes down the equation of motion for the correlation functions of the fermions. This, of course leads to an infinite hierarchy of equations which needs to be truncated. Several such truncation schemes are discussed in the literature in various contexts<sup>18–21</sup>. Here we truncate these equations by writing all four point correlators (for both fermion and mixed correlators) as a product of two point correlations by using Wick's theorem.

The Heisenberg equations for expectation of any operator  $\mathcal{O}_{\vec{k}}$  can then be written as

$$i\partial_t \langle \mathcal{O}_{\vec{k}} \rangle = \langle [H_{\text{total}}, \mathcal{O}_{\vec{k}}] \rangle \quad (25)$$

where the expectation is taken with respect to the initial state at  $t = 0$ . Here we shall choose this state to be a direct product state of fermions and the bath bosons  $|\psi\rangle_{\text{init}} = |\psi\rangle_{\text{fermion}} \otimes |\psi\rangle_{\text{bath}}$ . This procedure yields

$$\begin{aligned} i\partial_t n(\vec{k}) &= -\Delta_{\vec{k}} F^*(\vec{k}) + \Delta_{\vec{k}}^* F(\vec{k}) + \lambda_{\vec{k}} (A_1(\vec{k}, \vec{q}) + A_2(\vec{k}, \vec{q})) - \lambda_{\vec{k}-\vec{q}} (A_1(\vec{k} - \vec{q}, \vec{q}) + A_2(\vec{k} - \vec{q}, \vec{q})) \\ &\quad - \lambda_{\vec{k}} (A_1^*(\vec{k}, \vec{q}) + A_2^*(\vec{k}, \vec{q})) + \lambda_{\vec{k}-\vec{q}} (A_1^*(\vec{k} - \vec{q}, \vec{q}) + A_2^*(\vec{k} - \vec{q}, \vec{q})) \\ i\partial_t F(\vec{k}) &= 2(g(t) - z_{\vec{k}}) F(\vec{k}) + \Delta_{\vec{k}} ((n(\vec{k}) + n(-\vec{k})) - 1) + \lambda_{\vec{k}} (G_1(\vec{k}, \vec{q}) + G_2(\vec{k}, \vec{q})) \\ &\quad + \lambda_{-\vec{k}} (G_1(\vec{k} - \vec{q}, \vec{q}) + G_2(\vec{k} - \vec{q}, \vec{q})) + \lambda_{\vec{k}-\vec{q}} (G_1(\vec{k}, -\vec{q}) + G_2(\vec{k}, -\vec{q})) + \lambda_{\vec{k}-\vec{q}} (G_1(\vec{k} + \vec{q}, -\vec{q}) + G_2(\vec{k} + \vec{q}, -\vec{q})) \\ i\partial_t A_{1[2]}(\vec{k}, \vec{q}) &= (z_{\vec{k}} - z_{\vec{k}+\vec{q}}) A_{1[2]}(\vec{k}, \vec{q}) + \Delta_{\vec{k}+\vec{q}} G_{2[1]}^*(-\vec{k}, -\vec{q}) + \Delta_{\vec{k}}^* G_{1[2]}(\vec{k}, \vec{q}) - [+]\hbar\omega_{\vec{q}} A_{1[2]}(\vec{k}, \vec{q}) \\ &\quad + \lambda_{\vec{k}} (0[1] + n_b[+][-\omega_{\vec{q}}]) (n(\vec{k}) - n(\vec{k} + \vec{q})) - [+]\lambda_{\vec{k}} n(\vec{k} + \vec{q}) + [-]\lambda_{\vec{k}} n(\vec{k}) n(\vec{k} + \vec{q}) - [+]\lambda_{\vec{k}-\vec{q}} F^*(\vec{k}) F(\vec{k} + \vec{q}) \\ &\quad - i\gamma_0 A_{1[2]}(\vec{k}, \vec{q}) \\ i\partial_t G_{1[2]}(\vec{k}, \vec{q}) &= (2g(t) - z_{\vec{k}+\vec{q}} - z_{\vec{k}}) G_{1[2]}(\vec{k}, \vec{q}) + \Delta_{\vec{k}} A_{1[2]}(\vec{k}, \vec{q}) + \Delta_{\vec{k}+\vec{q}} A_{1[2]}(-\vec{k} - \vec{q}, \vec{q}) - [+]\omega_{\vec{q}} G_{1[2]}(\vec{k}, \vec{q}) \\ &\quad + (0[1] + n_b[+][-\omega_{\vec{q}}]) (\lambda_{\vec{k}} F(\vec{k}) + \lambda_{-\vec{k}-\vec{q}} F(\vec{k} + \vec{q})) + [-]\lambda_{-\vec{k}-\vec{q}} n(-\vec{k}) F(\vec{k} + \vec{q}) + [-]\lambda_{\vec{k}} F(\vec{k}) n(\vec{k} + \vec{q}) \\ &\quad - i\gamma_0 G_{1[2]}(\vec{k}, \vec{q}) \end{aligned} \quad (26)$$

where the terms  $\sim \gamma_0$  has been added to the equations of the correlators to counter numerical instability arising from truncation of the hierarchy as discussed earlier<sup>18,20</sup>. The correlators in Eq. 26 are given by

$$\begin{aligned} n(\vec{k}) &= \langle c_{\vec{k}}^\dagger c_{\vec{k}} \rangle, & F(\vec{k}) &= \langle c_{-\vec{k}} c_{\vec{k}} \rangle \\ A_1(\vec{k}, \vec{q}) &= \langle c_{\vec{k}}^\dagger c_{\vec{k}+\vec{q}} b_{\vec{q}}^\dagger \rangle, & A_2(\vec{k}, \vec{q}) &= \langle c_{\vec{k}-\vec{q}}^\dagger c_{\vec{k}} b_{-\vec{q}} \rangle \\ G_1(\vec{k}, \vec{q}) &= \langle c_{-\vec{k}} c_{\vec{k}+\vec{q}} b_{\vec{q}}^\dagger \rangle, & G_2(\vec{k}, \vec{q}) &= \langle c_{-\vec{k}} c_{\vec{k}+\vec{q}} b_{-\vec{q}} \rangle \end{aligned} \quad (27)$$

We note from Eq. 26 that the equations for the two point correlators such as  $n_{\vec{k}}$  and  $F_{\vec{k}}$  gives rise to higher order mixed correlators  $A_{1,2}(\vec{k}, \vec{q})$  and  $G_{1,2}(\vec{k}, \vec{q})$  which quantify correlations between electrons and phonons. These mixed correlators, in turn, give rise to four fermion terms which have been decomposed into lower order two point correlators using Wick's theorem as mentioned earlier. This leads to the closed set of equations (Eq. 26) which are solved numerically to study the dynamics.

## B. Numerical Results

The numerical solution of Eq. 26 allows us to obtain information about dynamics of both Ising and Kitaev models coupled to bosonic bath. For all numerical solutions used for results presented in this section, we have set  $\lambda_{\vec{k}} = \lambda$  for all  $\vec{k}$  and, unless otherwise mentioned, kept the phenomenological damping constant  $\gamma_0 = 0.2\lambda$ , where  $\lambda/J$  is considered to be the smallest scale in the problem. We have checked, by varying  $\gamma_0$  around this value, that the nature of the correlator remains independent of  $\gamma_0$  value in this regime. Also, for all plots, we have used a single bosonic mode at  $\vec{q} = \vec{q}_0 = (4\pi/L, 4\pi/L)$  (where  $L$  is the linear dimension of the system) for the Kitaev model,  $q = q_0 = 4\pi/L$  for the Ising model, and have set  $\hbar\omega_{q_0}/J = 20$  to be the largest scale in the problem. We have chosen a finite non-zero  $\vec{q}_0$  to ensure non-trivial coupling to the bath (for  $\vec{q} = 0$ ,  $[n_{\vec{k}}, H_1] = 0$ ) while  $\hbar\omega_{\vec{q}}/J \gg 1$  is chosen to ensure that neglecting back-reaction of the system on the bath remains a valid assumption.

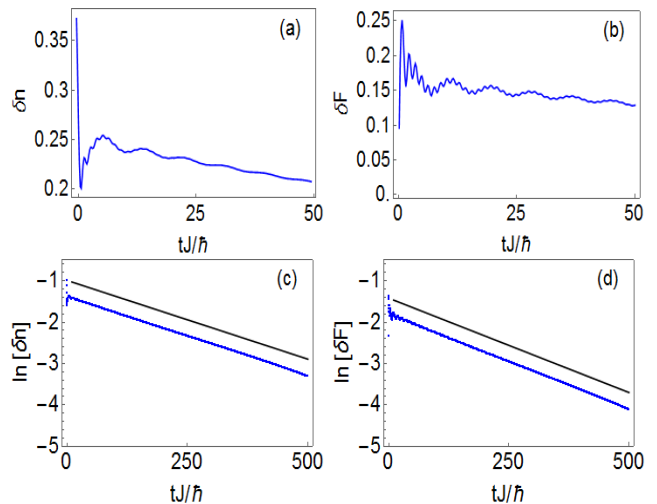


FIG. 9: (a) Evolution of  $\delta n$  as a function of time  $t$  (in units of  $\hbar/J$ ) for  $g_i/J = 2.5$ ,  $g_f = 0$ ,  $\lambda/J = 0.8$ , and  $\hbar\omega_D = 10\pi J$ . (b) Similar plot for  $\delta F$ . (c) Plot of  $\ln \delta n$  as a function of  $t$  over longer time scale showing the exponential decay of  $\delta n$  with time. The black line is the fit from which one obtains  $\hbar\mu_n = 0.0038J$ . (d) Similar plot for  $\ln \delta F$  with  $\hbar\mu_F = 0.0044J$ . See text for details.

The result for this numerical study is shown in Fig. 9 for the Ising model in a transverse field. Fig. 9(a),(b) shows the time variation the correlators  $\delta n = \sum_k (n_k - n_k^{\text{steady state}})$  and  $\delta F = \sum_k (F_k - F_k^{\text{steady state}})$  as a function of time  $t$  (in units of  $\hbar/J$ ). We find that the correlators shows a decaying behavior which sets in after brief oscillations for the first few cycles of the drive. The nature of this decay is shown in Fig. 9(c),(d). We find that, in contrast to fermionic bath, the presence of bosonic bath leads to an exponential decay of the correlators to their steady state value. The corresponding decay coefficients  $\mu_n$  (of  $\delta n$ ) and  $\mu_F$  (of  $\delta F$ ) are plotted as a function of the drive frequency  $\omega_D$  in Fig. 10. This plot indicates that  $\mu_n$  and  $\mu_F$  increases linearly with  $\omega_D$ . This in turn implies that the decay of the correlators as a function of number of drive cycles  $n_0$  is independent of  $\omega_D$ . Indeed, it is easy to see that if  $\delta n(\delta F) \sim \exp[-\mu'_{n(F)} n_0]$ , then  $\mu'_{n(F)} = \mu_{n(F)} T$  and  $\mu'_{n(F)}$  is thus independent of  $\omega_D$  for  $\mu_{n(F)} \sim \omega_D$ .

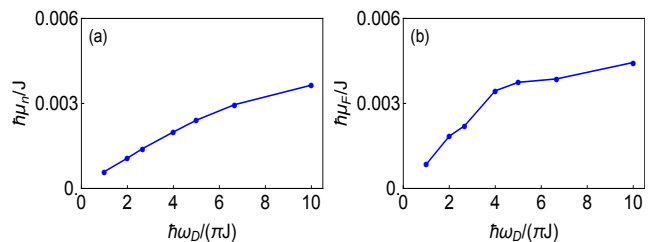


FIG. 10: (a) Plot of  $\mu_n$  as a function of  $\omega_D$  (in units of  $J/\hbar$ ) for  $g_i/J = 2.5$ ,  $g_f = 0$ ,  $\lambda/J = 0.8$ . (b) Similar plot for  $\mu_F$ . See text for details.

Next, we investigate the role of the coupling parameter  $\lambda$  behind such exponential decay of correlation functions. To this end, we note that the exponential decay of the correlation functions sets in at shorter time scales for larger  $\lambda$ ; indeed it is possible to define a critical number of drive cycles  $n_c$  at any drive frequency around which a crossover from power-law to exponential decay takes place. This can be seen from the plot of  $\delta n$  as a function of  $n_0$  in Fig. 11 where the crossover from power-law to exponential behavior occurs around  $n_0 \sim 800$ .

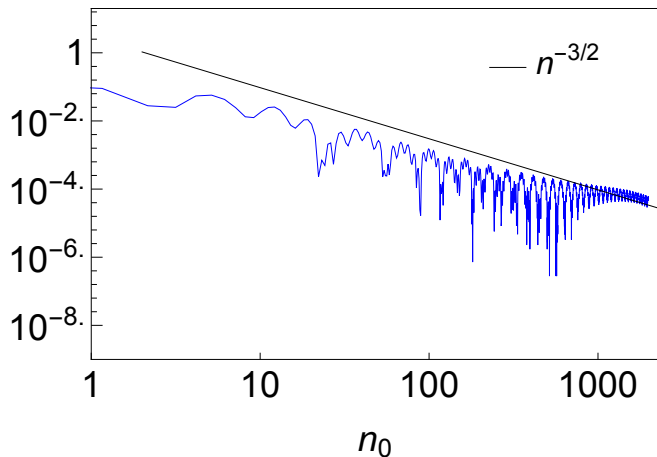


FIG. 11: Plot of  $\delta n$  as a function of  $n_0$  for  $g_i/J = 2.5$ ,  $g_f = 0$ ,  $\lambda/J = 0.04$ , and  $\hbar\omega_D/J = 10\pi$ . The plot shows the change for power law to exponential decay around  $n_c \simeq 800$ . See text for details.

For  $n_0 \ll n_c$ , the behavior of the system is analogous to a closed Ising chain and the correlators display dynamical transition as a function of frequency. For  $n_0 \geq n_c$ , the system shows the exponential decay shown in Fig. 11. A plot of  $n_c$  as a function of  $\lambda/J$  is shown in Fig. 12(a); we find that  $\delta n_c \sim 1/\lambda^2$ . This behavior can be understood as follows. We note that the integrability of the Ising chain is destroyed by scattering between different modes due to  $H_1 \sim \lambda$ ; thus a simple Fermi golden rule argument allows us to deduce that the time scale for such scattering to become relevant would be  $\sim 1/\lambda^2$ . This behavior is qualitatively similar to that of Fermi-Pasta-Ulam chain<sup>22</sup> where it was shown that a finite strength of integrability-breaking term is necessary to destroy the integrable nature of the correlation functions. A plot of  $n_c$  as a function of  $g_f/J$  for a fixed  $\lambda/J$  is shown in Fig. 12(b). The plot indicates that integrability breaking behavior sets in more quickly for larger amplitude quenches. This can be understood by considering the fact that larger amplitude quenches amounts to larger energy transfer to the system which can lead to quicker access to the bath degrees of freedom.

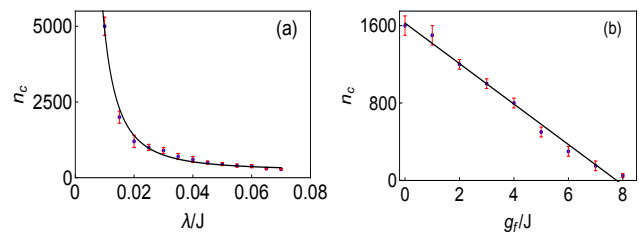


FIG. 12: (a) Plot of  $n_c$  as a function of  $\lambda$  (in units of  $J$ ) for  $g_i/J = 2.5$ ,  $g_f = 0$ ,  $\hbar\omega_D/J = 10\pi$ . The lines shows a  $1/\lambda^2$  fit to the data points indicated by circles. (b) Plot of  $n_c$  as a function of  $g_f$  for  $\lambda = 0.8J$ . All other parameters are same as in (a). See text for details.

Next we address the dynamics of the Kitaev model. For this, we scale all quantities by  $J_1$  and set  $J_2 = J_1$ ,  $\hbar\omega_D = 20J_1$ . For all numerics,  $J_3$  is varied using a square pulse protocol between  $J_{3i} = 2.5J_1$  and  $J_{3f} = 0$  with a frequency  $\omega_D$ . In Fig. 13, we show the dynamics of  $\ln \delta n$  and  $\ln \delta F$  for the Kitaev model as a function of time  $t$  (in units of  $\hbar/J_1$ ). The decay is again found to be exponential as can be inferred from Fig. 13.

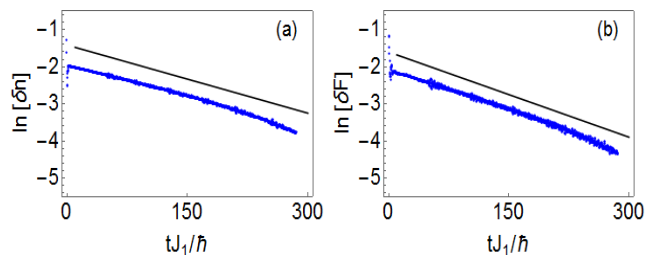


FIG. 13: (a) Plot of  $\ln \delta n$  as a function of  $t$  (in units of  $\hbar/J_1$ ) for  $J_{3f}/J_1 = 4$ ,  $J_{3i}/J_1 = 5$ ,  $\lambda/J_1 = 0.8$ ,  $\gamma_0/\lambda = 0.2$ , and  $\hbar\omega_D = 10\pi J_1$ . The black line denotes the fit which yields  $\hbar\mu_n^K = 0.0062J_1$ . (b) Similar plot for  $\ln \delta F$  with  $\hbar\mu_F^K = 0.0072J_1$ . See text for details.

The decay coefficients of the correlation functions  $\mu_n^K$  and  $\mu_F^K$  for the Kitaev model is shown in Fig. 14. These plots indicates that both  $\mu_n$  and  $\mu_F$  for the Kitaev model show an almost linear variation with drive frequency similar to those for the Ising model. This in turn indicates that  $\mu_{n,F}^K$  would be almost independent of  $\omega_D$ . The variation of  $n_c$  as a function of  $\lambda$  shown in Fig. 15 is also qualitatively similar to that for the 1D Ising model. This seems to suggest that such behavior of  $n_c$  is quite general and one may expect to observe a dynamic transition for open systems at sufficiently small  $\lambda$ ; similar behavior is also expected to be observed for CDW and superconducting systems.

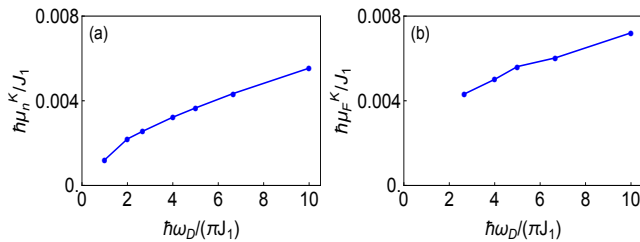


FIG. 14: (a) Plot of  $\mu_n$  as a function of  $\omega_D$  (in units of  $J_1/\hbar$ ) for  $J_{3f}/J_1 = 4$ ,  $J_{3i}/J_1 = 5$ , and  $\lambda/J_1 = 0.8$ . (b) Similar plot for  $\mu_F$ . All other parameters are same as in Fig. 13. See text for details.

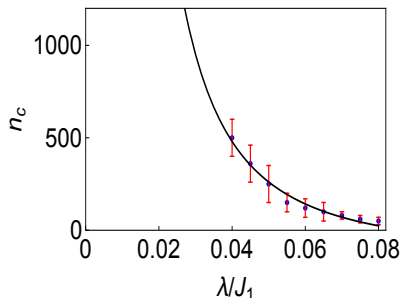


FIG. 15: Plot of  $n_c$  as a function of  $\lambda$  (in units of  $J_1$ ) for  $J_{3f}/J_1 = 4$ ,  $J_{3i}/J_1 = 5$ , and  $\hbar\omega_D/J_1 = 10\pi$ . The dots represents data points where the black line shows  $1/\lambda^2$  fit to the data. All other parameters are same as in Fig. 13. See text for details.

#### IV. DISCUSSION

In this work, we have studied the dynamics of a class of driven integrable models coupled to an external bath. These models exhibit drive frequency induced dynamical transitions in the absence of the bath<sup>9,10</sup>; our focus in this work has been to study the fate of this dynamical transition in the presence of external baths. Our study, which constitutes a generalization of such transition to open quantum systems, reveals that the fate of such transitions crucially depends on whether the bath breaks integrability of the closed system.

For fermionic baths with linear coupling, where the integrability of the closed system remains intact, we find that the transition survives. For such baths, we provide a semi-analytic expression for the Floquet eigenvalues corresponding to a square pulse drive protocol. Using this, we chart out the different dynamical phases of the system coupled to a fermionic bath. We demonstrate that the coupling parameter between the system and the bath,  $\lambda$ , can induce a new class of dynamical transitions which occur at large  $\lambda$ . We note that such transitions occur at high drive frequencies where the closed system exhibits  $n_0^{-d+1/2}$  decay; thus they do not have any analogue for

closed integrable systems studied earlier. In particular, we find transition lines in the  $\eta - \lambda$  plane for a fixed drive frequency; this demonstrates the possibility of tuning these transition by varying fermionic bath parameters.

In contrast, for bosonic baths which destroy the integrability of the model, we use an equation of motion technique to study the dynamics. We restrict ourselves to the limit where the backreaction of the system on the bath can be ignored. In this regime, we find that all correlators decay to their steady state value exponentially; these decays are characterized by decay coefficients which varies linearly with the drive frequency for the 1D Ising model and 2D Kitaev model. We note that such a decay sets in after a critical number of drive cycles  $n_c$ ; for  $n_0 \ll n_c$ , the power law decay of the closed system survives. We chart out  $n_c$  as a function of the coupling strength  $\lambda$  and show that  $n_c \sim 1/\lambda^2$ . This result indicates that for weak enough system-bath coupling strength, one expects a large time window where the dynamical transition would survive. We note that this result also holds for weakly interacting closed fermion systems whose kinetic term is given by  $H_0$ . This is seen by noting that our analysis for the bosonic bath is carried out for  $\hbar\omega_{\vec{q}}/J \gg 1$ ; in this regime integrating out the bath degrees of freedom leads to a density-density interaction term for the fermions with strength  $\sim \lambda^2/(\hbar\omega_{\vec{q}_0})$ .

Possible experimental platforms which can emulate such models involves ultracold atom setups<sup>23,24</sup> or quantum dots<sup>25,26</sup>. In particular, in Ref. 24, Dirac fermions described by  $H_0$  was experimentally realized by emulating fermions on a honeycomb lattice such as the one found in graphene. The bosonic bath may be realized by coupling such a system to bath of oscillators; this was done for bosonic condensates earlier<sup>27</sup>. For fermionic bath, the setup in Ref. 24 may be coupled to another 2D square lattice which host fermions with tight binding dispersion. We propose measurement of expectation of fermion density  $n = \langle \sum_{\vec{k}} \psi_{\vec{k}}^\dagger \psi_{\vec{k}} \rangle$  as a function of time in such composite systems to verify the presence of two different dynamical regimes.

In conclusion, we have studied driven dynamics of a class of integrable fermionic models coupled to either fermionic or bosonic baths. We have charted out the dynamical phases of these systems as a function of drive frequency and system-bath parameters. Our results show that the effect of these baths on the driven system depends crucially on whether they preserve the integrability of the system. We have discussed experiments which can test our results.

#### Acknowledgments

The authors thank A. Sen and R. Ghosh for discussion.

- <sup>1</sup> A. Polkovnikov, K. Sengupta, A. Silva, and M. Vengalattore, *Rev. Mod. Phys.* **83**, 863 (2011); J. Dziarmaga, *Adv. Phys.* **59**, 1063 (2010); A. Dutta, G. Aeppli, B. K. Chakrabarti, U. Divakaran, T. F. Rosenbaum, and D. Sen, *Quantum phase transitions in transverse field spin models: from statistical physics to quantum information* (Cambridge University Press, Cambridge, 2015); S. Mondal, D. Sen and K. Sengupta, *Non-equilibrium dynamics of quantum systems: order parameter evolution, defect generation, and qubit transfer*, *Lect. Notes Phys.* **21** 802 (2010).
- <sup>2</sup> M. Bukov, L. D'Alessio, and A. Polkovnikov, *Adv. Phys.* **64** 139 (2015); L. D'Alessio and A. Polkovnikov, *Ann. Phys.* **333**, 19 (2013).
- <sup>3</sup> T. Kitagawa, E. Berg, M. Rudner, and E. Demler, *Phys. Rev. B* **82**, 235114 (2010); N. H. Lindner, G. Refael, and V. Galitski, *Nat. Phys.* **7**, 490 (2011); T. Kitagawa, T. Oka, A. Brataas, L. Fu, and E. Demler, *Phys. Rev. B* **84**, 235108 (2011); F. Nathan and M. S. Rudner, *New J. Phys.* **17** 125014 (2015); B. Mukherjee, A. Sen, D. Sen, and K. Sengupta, *Phys. Rev. B* **94**, 155122 (2016); B. Mukherjee, P. Mohan, D. Sen, and K. Sengupta, *Phys. Rev. B* **97**, 205415 (2018).
- <sup>4</sup> A Lazarides, A Das, R Moessner, *Phys. Rev. E* **90**, 012110 (2014); A. Russomanno, A. Silva, and G. E. Santoro *Phys. Rev. Lett.* **109**, 257201 (2012).
- <sup>5</sup> For a review, see F. Harper, S. Roy, M. S. Rudner, and S. L. Sondhi, *Annual Review of Condensed Matter Physics* **11**, 345 (2020).
- <sup>6</sup> A. Das, *Phys. Rev. B* **82**, 172402 (2010); S. S. Hegde, H. Katiyar, T. S. Mahesh, and A. Das, *ibid.* **90**, 174407 (2014); S. Mondal, D. Pekker, and K. Sengupta, *Europhys. Lett.* **100**, 60007 (2012); U. Divakaran and K. Sengupta, *Phys. Rev. B* **90**, 184303 (2014); B. Mukherjee, A. Sen, D. Sen, and K. Sengupta, arXiv:2005.07715 (unpublished).
- <sup>7</sup> B. Mukherjee, S. Nandy, A. Sen, D. Sen, and K. Sengupta, *Phys. Rev. B* **101**, 245107 (2020); B. Mukherjee, A. Sen, D. Sen, and K. Sengupta, arXiv:2002.08683 (unpublished).
- <sup>8</sup> For a review, see M. Heyl, *Rep. Prog. Phys.* **81**, 054001 (2018).
- <sup>9</sup> A. Sen, S. Nandy, and K. Sengupta, *Phys. Rev. B* **94**, 214301 (2016).
- <sup>10</sup> S. Nandy, K. Sengupta, and A. Sen, *J. Phys. A: Math. Theor.* **51**, 334002 (2018).
- <sup>11</sup> S. Sachdev, *Quantum Phase Transitions* (Cambridge University Press, Cambridge, 1999).
- <sup>12</sup> P. Wang, S. Lin, G. Zhang, Z. Song, *Sci Rep* **7**, 17179 (2017).
- <sup>13</sup> A. Kitaev, *Ann. Phys.* **321**, 2 (2006); H-D Chen and Z. Nussinov, *J. Phys. A: Math. Theor.* **41**, 075001 (2008).
- <sup>14</sup> K. Seetharam, C. Bardyn, N. Lindner, M. Rudner, G. Refael, *Phys. Rev. X* **5**, 041050 (2015). ; K. Seetharam, C. Bardyn, N. Lindner, M. Rudner, G. Refael, *Phys. Rev. B* **99**, 014307 (2019).
- <sup>15</sup> R. Ghosh, N. Dupuis, A. Sen and K. Sengupta, *Phys. Rev. B* **101**, 245130 (2020).
- <sup>16</sup> See for example, J. W Negele and H. Orland, *Quantum Many-particle Systems*, *Frontiers in Physics* (1998).
- <sup>17</sup> See, for example, H-P. Breuer and F. Petruccione, *The theory of open quantum systems*, Oxford University Press (2002).
- <sup>18</sup> See, for example Echehard Scholl, *Theory of Transport Properties of Semiconductor Nanostructures*, Springer Science (1998).
- <sup>19</sup> See, for example M. Kira, S. Koch, *Semiconductor Quantum Optics*, Cambridge Univ. Press (2012).
- <sup>20</sup> I. Savic, N. Vukmirovic, Z. Ikonc et al., *Phys. Rev. B* **76**, 165310 (2007).
- <sup>21</sup> S. Butscher, J. Forstner, I. Waldmuller, A. Knorr, *Phys. Rev. B* **72**, 045314 (2005).
- <sup>22</sup> E. Fermi, J. Pasta, and S. Ulam, Los Alamos Report LA-1940, (1955); *Collected works of E. Fermi*, Ed. E. Serge, Vol. II (University of Chicago Press, 1965); For a review see, G. P. Berman and F. M. Izrailev, *Chaos* **15**, 015104 (2005).
- <sup>23</sup> I. Bloch, J. Dalibard, and W. Zwerger, *Rev. Mod. Phys.* **80**, 885 (2008)
- <sup>24</sup> L. Tarruell, D. Greif, T. Uehlinger, G. Jotzu, and T. Esslinger, *Nature* **483**, 302 (2012).
- <sup>25</sup> T. Hensgens et al, *Nature* **548** 70-73 (2017).
- <sup>26</sup> S. Mostame and Ralf Schutzhold, *Phys. Rev. Lett.* **101**, 220501 (2008).
- <sup>27</sup> P. Treutlein, D. Hunger, S. Camerer, T. W. Hansch, and J. Reichel *Phys. Rev. Lett.* **99**, 140403 (2007); D. Hunger, S. Camerer, T. W. Hansch, D. Konig, J. P. Kotthaus, J. Reichel, and P. Treutlein, *Phys. Rev. Lett.* **104**, 143002 (2010).